Applied Physics B (2020) 126:44
https://doi.org/10.1007/s00340-020-7385-7

Applied Physics B
Lasers and Optics

Spectroscopy and diode-pumped continuous-wave laser operation of Tm:Y_2O_3 transparent ceramic at cryogenic temperatures

Fangxin Yue[1,2,3] · Venkatesan Jambunathan[1] · Samuel Paul David[1] · Xavier Mateos[2] · Magdalena Aguiló[2] · Francesc Díaz[2] · Jan Šulc[3] · Antonio Lucianetti[1] · Tomáš Mocek[1]

Received: 14 October 2019 / Accepted: 23 January 2020 / Published online: 19 February 2020

Abstract
We present the spectroscopic and laser characteristics of a 3 at.% Tm:Y_2O_3 transparent ceramic at cryogenic temperatures. An absorption cross section of 4.7×10^{-21} cm^2 with a bandwidth of 0.7 nm centered at 793.3 nm and an emission cross section of 29.0×10^{-21} cm^2 centered at 1930.9 nm were estimated at 80 K. Continuous-wave laser operation was achieved using broadband and VBG stabilized laser diodes emitting around 793 nm as pump sources. With the VBG pump diode, a maximum output power of 6.4 W was achieved at 80 K corresponding to a slope efficiency of 52.0% with respect to absorbed power.

1 Introduction

Emerging applications, such as laser-induced damaged threshold measurement, polymer material processing, debris removal from space, pump source for Mid-Infrared (Mid-IR) lasers, including ultrafast optical parametric oscillators based on non-oxide nonlinear crystals, etc., require compact high average and peak power (HAPP) laser sources emitting at the two-micron spectral range [1–4]. In this aspect, two kinds of rare earth ion-doped active materials are preferred: thulium (Tm^{3+})-doped active materials (typically emitting at slightly shorter than two microns) and holmium (Ho^{3+})-doped active materials (emitting at slightly longer than two microns). Both active ions have their own merits and demerits. However, in this work, we give more emphasis on the former one.

The $^3H_6\rightarrow{}^3H_4$ transition in Tm absorbs effectively around 793 nm, which can be directly pumped by the commercially available AlGaAs laser diodes emitting at 793 nm. This also increases the compactness of the laser setup. In addition, one important advantage of the Tm-doped materials is that they experience the so-called two-for-one cross-relaxation mechanism, meaning that, a pump photon can excite two Tm ions in the $^3F_4$ emitting level [5]. This will result in much higher slope efficiency (~80%) than the quantum defect limited value (~40%) [6].

However, Tm ions suffer from reabsorption losses due to the quasi-three level absorption–emission transitions at room temperature and, in addition, they suffer from other parasitic processes such as excited state absorption (ESA) and energy-transfer upconversion (ETU), limiting the power scaling capabilities and hindering to achieve high beam quality [7]. To mitigate these issues, cooling the active medium down to cryogenic temperatures is a proper solution. Cryogenic cooling increases the thermal conductivity and transition cross sections of the laser active materials, while reduces their thermal expansion and thermo-optic coefficients, which are prerequisites for the development of HAPP lasers [8].

Among Tm-doped active media, crystalline thulium-doped yttrium oxide (Tm:Y_2O_3), belonging to the sesquioxide family, stands out because of its very high thermal conductivity (13.4 W/mK at room temperature for undoped Y_2O_3 [9]), broad emission bandwidth and a relatively low maximum phonon energy (597 cm^{-1} [9]), which make it suitable for two-micron laser operation in several temporal regimes [10, 11]. However, the high melting point of

✉ Venkatesan Jambunathan
jambunath@fzu.cz

1 HiLASE Center, Institute of Physics Czech Academy of Sciences, Za Radnicí 828, 25241 Dolní Břežany, Czech Republic

2 Física i Cristal·lografia de Materials i Nanomaterials (FiCMA-FiCNA), Universitat Rovira i Virgili, Campus Sescelades, c/Marcel·lí Domingo, s/n., 43007 Tarragona, Spain

3 Faculty of Nuclear Sciences and Physical Engineering, Czech Technical University in Prague, Brehova 7, 115 19 Prague, Czech Republic

$Tm:Y_2O_3$ is the main limitation in its crystal growth process. Achieving high-quality crystals of large size becomes a tedious and expensive task. This important limitation is overcome by transparent ceramic fabrication process. Several works have been reported based on Tm-doped sesquioxide ceramics [12–14]. To the best of our knowledge, no studies on cryogenic $Tm:Y_2O_3$ have been reported yet either in crystalline or ceramic form.

Based on the above-mentioned facts, this work is mainly devoted to study the spectroscopic properties of $Tm:Y_2O_3$ transparent ceramics at cryogenic temperatures. This study helps not only to understand the spectroscopic characteristics of $Tm:Y_2O_3$ at cryogenic temperatures but also to determine the crucial laser design parameters for HAPP lasers, such as the exact pump wavelength, absorption bandwidth, small signal gain, amplified spontaneous emission estimation, etc. Besides, we also studied the continuous-wave laser performance of this material at cryogenic temperatures using both broadband and VBG stabilized laser diodes as the pump source.

2 Experimental

2.1 Cryogenic spectroscopy setup

The cryogenic spectroscopic characterizations comprise of absorption and photoluminescence measurements, which were carried out from room temperature down to 6 K in step size of 20 K. To achieve cryogenic temperatures, the sample was mounted in an aluminum holder and cooled by a Leybold helium closed cycle cryostat. For the absorption measurements, a spectrophotometer (*Cary 5000 UV–Vis–NIR*) was used. In the photoluminescence measurements, the sample was excited using an un-polarized broadband diode laser emitting around 793 nm. The photoluminescence was collected and then fiber was coupled (600 µm, N.A. = 0.39) to the optical spectrum analyzer (*AQ6375B, YOKOGAWA*) with a spectrum resolution of 0.5 nm.

For lifetime measurements, the sample was pulsed pumped under an angle, so that the effect of reabsorption was reduced [15]. The pulse duration was 10 ms in 20-Hz repetition rate and 20% duty cycle. The time decay of the $^3F_4$ level of Tm ions was measured for different temperatures by a PbS detector (*PDA30G-EC, Thorlabs*), and a long pass filter was used to block the pump radiation passing through the detector. Then, the signal was collected and averaged by a digital oscilloscope (*WaveSurfer 64MXs-B, Teledyne LeCroy*). The values of absorption, emission and gain cross sections (σ_a, σ_e and σ_g) were determined using the theoretical approach based on Lambert–Beer's law, reciprocity and Fuchtbauer-Ladenburg (FL) methods, respectively [16–18].

2.2 Cryogenic continuous-wave (CW) laser setup

Figure 1 illustrates the schematic diagram of the cryogenic continuous-wave (CW) laser setup. The ~ 77-cm-long L-shape asymmetric cavity includes a plano-concave mirror M1 (radius of curvature ROC = − 300 mm), a dichroic mirror M2, a plano-convex lens L3 (f = 150 mm) and a plane output coupler M3. M1 is high-reflectively (HR) coated for 1800–2200 nm. The rear side of M2 is anti-reflectively (AR) coated at the pump wavelength range and front side is HR coated for the laser wavelength range. The lens L3 is broadband AR coated for the laser wavelength. As the output coupler (M3), different transmissions (T_{oc}) of 5, 9, 15, 20 and 30% were used. Two kinds of diode lasers emitting around 793 nm were used as pump sources, one with a broad bandwidth ($\Delta\lambda_P$ ~ 3 nm) and the other with a bandwidth of 0.5 nm stabilized by a Volume Bragg Grating (VBG). Both diodes are coupled by a fiber of core diameter of 105 µm and N.A. = 0.22 delivering a maximum output power of 30 W and 25 W, respectively. The radiation from the pump source was imaged to the active medium in 1:2 ratio by two AR-coated achromatic lenses (L1 and L2, focal lengths of 100 and 200 mm, respectively). The pump spot size is ~ 210 µm in the active medium.

The active medium was placed at normal incidence to the pump radiation and was mounted in a copper holder in a vacuum chamber. To avoid condensation on the sample surface while cooling, the chamber was maintained at a vacuum pressure of 10^{-5} mbar. The cryogenic temperature of the active medium was achieved by a closed cycle helium cryostat (CH-204, JANIS), which can provide a cooling power of 13.5 W at 100 K. A Lake Shore temperature controller (DT 670) was used to monitor and maintain the sample temperature, which includes 2 silicon diode sensors and a 50 Ω heater.

For both the spectroscopy and laser experiments, a commercial uncoated 3 at.% $Tm:Y_2O_3$ transparent ceramic

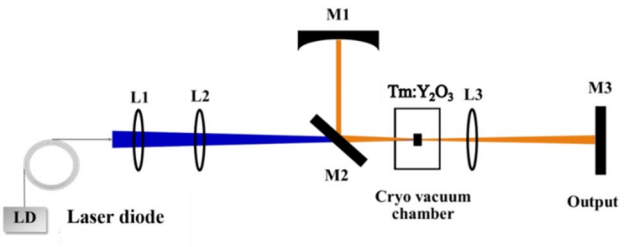

Fig. 1 Laser setup: LD—laser diode emitting at ~ 793 nm, core diameter 105 µm, N.A. = 0.22; L1 & L2—achromatic lenses (f_1 = 100 mm and f_2 = 200 mm); M1—concave cavity mirror (− 300 mm radius of curvature); M2—dichroic mirror; L3—plano-convex thin lens (f = 150 mm); M3—output coupler

($N_{Tm} = 7.96 \times 10^{20}$ atoms/cm^3) with thickness of 3 mm and diameter of 10 mm from *Konoshima Chemical Co., Ltd.* was employed.

3 Results and discussion

3.1 Cryogenic optical absorption cross sections

The absorption measurements were carried out for several manifolds and for various temperatures. For the sake of brevity, only selected absorption results at 750–850 nm ($^3H_6 \rightarrow {}^3H_4$ transition of Tm^{3+}) and 1500–2100 nm ($^3H_6 \rightarrow {}^3F_4$) ranges (as shown in Fig. 2a, b) were presented in this work, which are directly related to the absorption and emission bands involved in the laser excitation/generation, respectively. For both transitions, the peak values of absorption cross sections increase with the decrease of temperature, while the bandwidths are narrowed. A maximum absorption cross section of 14.1×10^{-21} cm^2 is observed at 40 K for the central wavelength of 775.8 nm, which is four times of that at room temperature.

Although several absorption peaks are available for pumping, the most interesting ones are those at 793 nm and 797 nm because of their larger cross sections and the possibility to be excited by the commercially available AlGaAs laser diodes. The absorption parameters for the laser design are presented in Table 1 for those two peaks at various temperatures, such as the central wavelength (λ_o), bandwidth ($\Delta\lambda$) and cross section (σ_a). From the table, no significant shift of the central wavelength can be observed when the temperature varies from 300 to 80 K; whereas, the bandwidths of both peaks narrow down to <1 nm. The maximum absorption cross sections amount to 4.7 and 6.5×10^{-21} cm^2 (at 80 K) for both peaks, respectively.

3.2 Cryogenic emission and gain cross sections

The cryogenic emission cross sections at various temperatures in the 1550–2200 nm wavelength region, corresponding to the $^3F_4 \rightarrow {}^3H_6$ transition, were estimated by combining both the reciprocity and FL methods. The methodology used to estimate the combined emission cross sections is the same as described in our previous works [15, 19]. Table 2 shows the data used for calculation of emission cross sections.

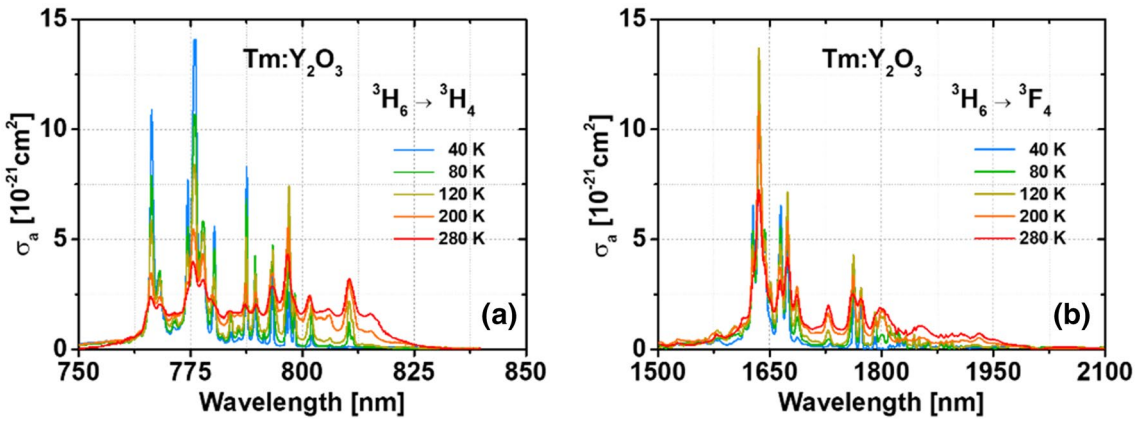

Fig. 2 Temperature dependence of absorption cross sections **a** in the 750–850-nm region ($^3H_6 \rightarrow {}^3H_4$ transition), **b** in the 1500–2100 nm region ($^3H_6 \rightarrow {}^3F_4$ transition)

Table 1 Absorption parameters for laser design

Temp (K)	793-nm peak			797-nm peak		
	λ_o (nm)	$\Delta\lambda$ (nm)	σ_a (10^{-21} cm^2)	λ_o (nm)	$\Delta\lambda$ (nm)	σ_a (10^{-21} cm^2)
80	793.3	0.7	4.7	797.1	0.6	6.5
120	793.3	1.1	4.5	797.0	0.7	7.4
160	793.3	1.3	3.8	796.9	0.9	6.6
200	793.3	1.4	3.5	796.8	1.1	5.6
240	793.3	1.8	3.2	796.7	1.4	4.8
280	793.4	2.3	2.9	796.7	1.4	4.3
300	793.4	2.4	2.8	796.6	1.8	3.9

Table 2 Data used for estimation of emission cross sections with the reciprocity and FL methods

	$Tm:Y_2O_3$	References
$^3H_6$ level splitting (cm^{-1})	0, 31, 89, 219, 230, 340, 382, 436, 488, 692, 788, 797	[20]
$^3F_4$ level splitting (cm^{-1})	5615, 5674, 5780, 6005, 6018, 6114, 6144, 6189	[20]
λ_{zl} (nm)—zero phonon line	1781	[20]
Z_l/Z_u	1.31 (80 K), 1.39 (160 K), 1.46 (240 K), 1.48 (280 K)	
τ (ms)—luminescence lifetime	3.5	[7]
n—Refractive index @ 2 μm	1.87	[21]

As shown in Fig. 3a, the peak values of the emission cross sections increase and bandwidths narrow down with the decrease of the sample temperature. The maximum emission cross section of 37.4×10^{-21} cm^2 at 1930.9 nm for 40 K was estimated, which is almost 4 times of that at room temperature. Near the liquid nitrogen temperature (~ 80 K), the maximum emission cross section amounts to 29.0×10^{-21} cm^2, which is still more than three times of the value at room temperature. In addition, we also determined the fluorescence decay time of the emitting level for the 3 at.% $Tm:Y_2O_3$ at various temperatures, which are shown in Fig. 3b. The obtained luminescence lifetimes are in the 3.1–3.6 ms range, which are close to the reported value of 3.5 ms [7].

Amplification of light is expected when the emission is higher than the absorption at the same wavelength for a given population ratio (β). In this aspect, one can estimate the gain cross sections using the equation $\sigma_g = \beta\sigma_e - (1-\beta)\sigma_a$, where σ_e is the emission cross section, σ_a is the absorption cross section. Figure 4a shows the estimated gain cross sections for various temperatures with fixed population ratio of $\beta = 0.1$. Figure 4b shows the estimated gain cross sections of different population ratios with fixed temperature (80 K). From Fig. 4a, one can infer that the gain cross section increases with a decrease in temperature for a given β. The highest gain peak is centered at ~ 1930 nm for temperatures lower than 240 K. For higher temperatures, the gain shifts to longer wavelength around 2050 nm. From Fig. 4b, one can infer that for a fixed sample temperature of 80 K, the gain cross section increases with the increase of β. The gain peak is centered at ~ 1930 nm. According to these estimations, one can expect a laser oscillation around 1930 nm at 80 K irrespective of the losses in the cavity. In addition, one can estimate the small signal gain coefficient g from the equation $g = \sigma_g \cdot N_{Tm}$, where N_{Tm} is the Tm concentration and σ_g is the gain cross section.

3.3 Cryogenic continuous-wave laser operation of $Tm:Y_2O_3$

As mentioned in the experimental section, the cryogenic CW laser operation was achieved by employing two different pump lasers emitting around 793 nm. The one with broadband emission ($\Delta\lambda_P$ ~ 3 nm) shows strong wavelength dependence on the diode operating current and the heat sink temperature (Fig. 5a—dashed lines). The VBG stabilized pump diode ($\Delta\lambda_P$ ~ 0.5 nm) shows almost no wavelength deviation (Fig. 5b—dashed lines). In addition, Fig. 5 (solid lines) illustrates the wavelength dependent absorption cross-section peaks of $Tm:Y_2O_3$ around 793 nm for various temperatures.

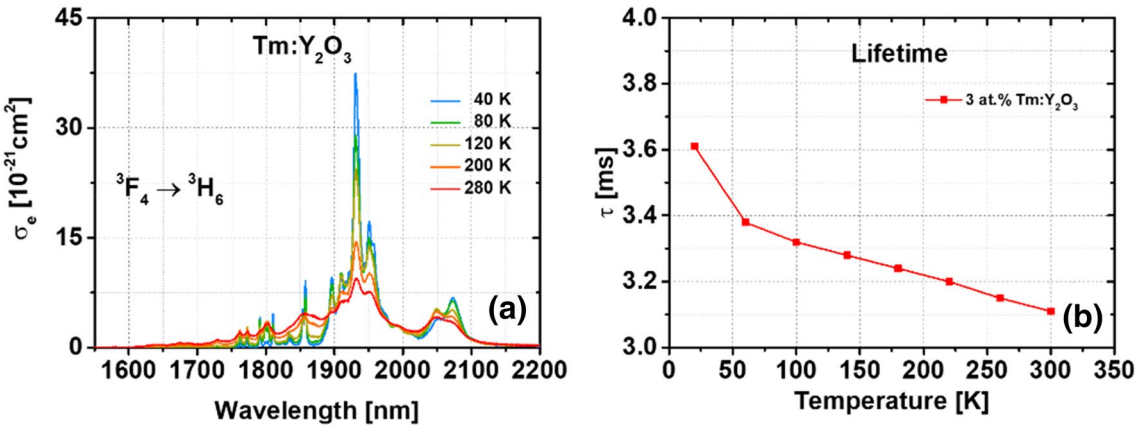

Fig. 3 **a** Emission cross sections in the 1600–2200-nm spectral range for various temperatures; **b** measured fluorescence lifetimes for various temperatures

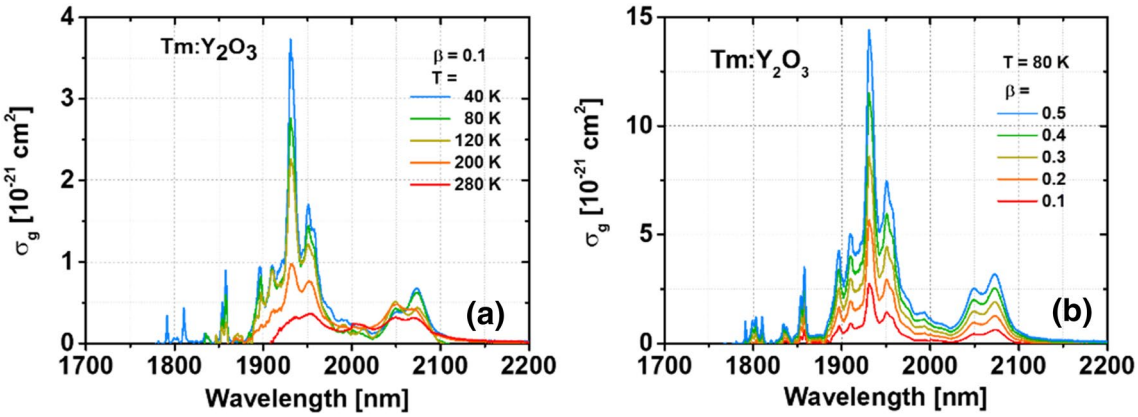

Fig. 4 Gain cross sections in the 1700–2200-nm range **a** for various temperatures with fixed $\beta = 0.1$ and **b** for different β values with temperature fixed at 80 K

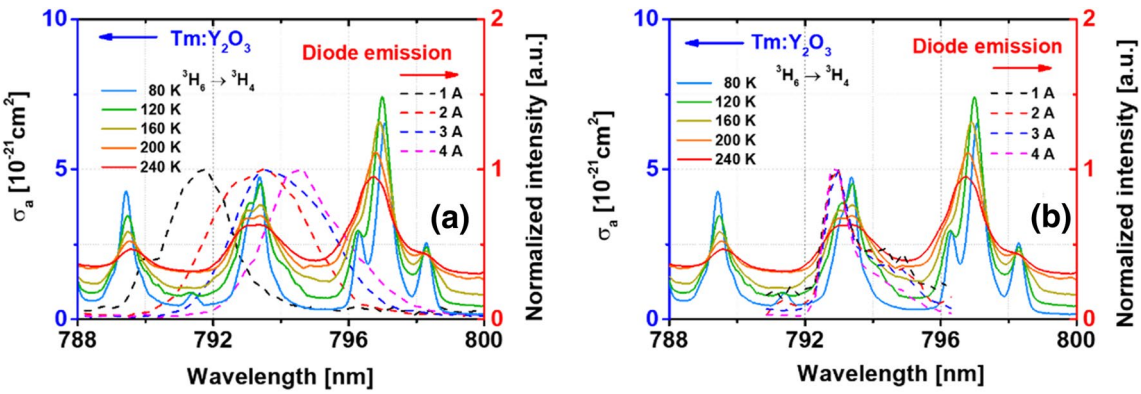

Fig. 5 Dashed lines: emission spectra around 793 nm of **a** the broadband diode and **b** the VBG stabilized diode at various diode currents. Solid lines: Tm:Y_2O_3 absorption peaks in around 793 nm at various temperatures

In the first set of experiments, CW lasing was characterized using the broadband pump diode. Its heat sink temperature was fixed to 25 °C. As shown in Fig. 6a, the sample temperature was firstly fixed to 80 K and the transmission of the output coupler was varied from 5 to 30%. In the incident/output characteristics, the incident power was measured after the dichroic mirror (M2). From the figure, one can observe that the linear dependence is lost for the incident power > 15 W. This is mainly due to the mismatch between the absorption band of Tm:Y_2O_3 and the pump emission band of the diode when the operating current was increased (Fig. 5a). Besides, only part of the pump is absorbed by the sample due to the narrow absorption band (0.7 nm at 80 K). A maximum output power of 2.2 W with a slope efficiency of 16.4% was achieved using output coupler of $T_{oc} = 30\%$.

However, increasing the sample temperature from 80 K up to 120 K results in a better slope efficiency (as shown in Fig. 6b). This indicates a better absorption of the pump power at higher temperatures due to the increase of the absorption bandwidth (see Table 1). The absorption in non-lasing condition was around 25% at 120 K pumped by the broadband diode. From this preliminary laser results, the importance of matching the wavelength and bandwidth of the sample absorption and the pump emission is confirmed. At higher temperatures, the decrease of absorption cross sections and thermal effects result in a drop of the slope efficiency.

To improve the laser results, a VBG stabilized diode at 793 nm maintained at 35 °C was employed as the pump source. The CW lasing was realized by varying two parameters: the output coupler transmission and the sample temperature. Figure 7a presents the laser incident/output power characteristics, when the output coupler transmission varied (5, 9, 15, 20 and 30%) and the sample temperature was fixed at 80 K. From the figure, a linear increase of the output power with respect to the incident power is observed without any thermal roll-over. A maximum output power of 6.4 W corresponding to a slope efficiency of 32.2% was achieved for $T_{oc} = 30\%$. This better performance of our laser using higher T_{oc}'s indicates that the parasitic processes are less

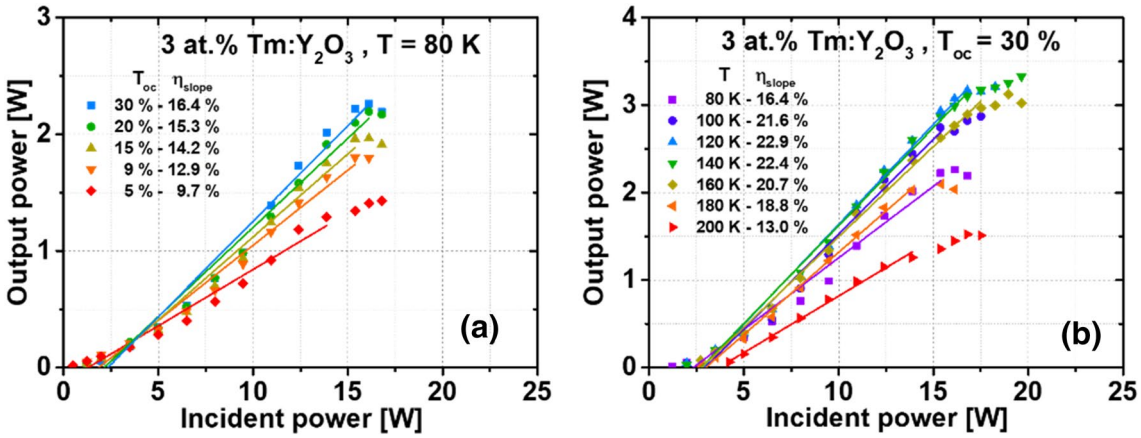

Fig. 6 Incident/output characteristics and slope efficiencies of the 3 at.% Tm:Y_2O_3 transparent ceramic laser pumped by broadband diode **a** at 80 K for various output coupler transmissions and **b** for various sample temperatures with $T_{oc} = 30\%$

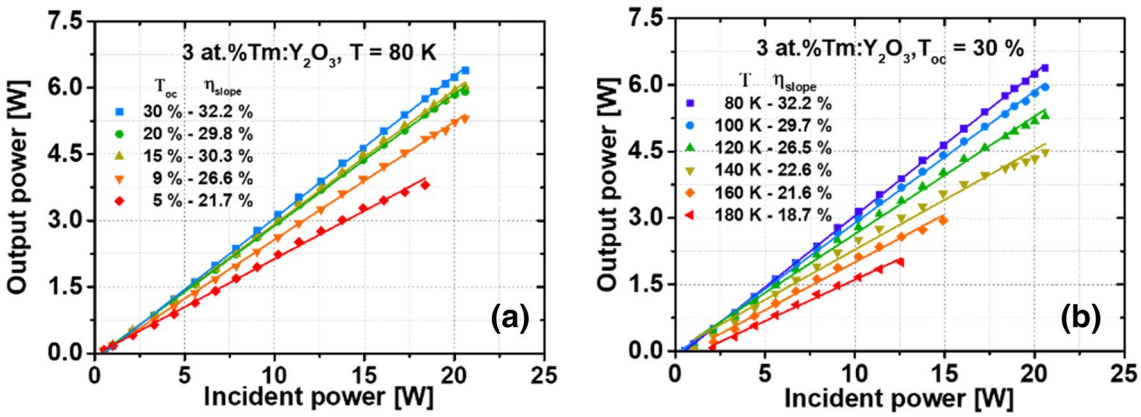

Fig. 7 Incident/output characteristics and slope efficiencies of 3 at.% Tm:Y_2O_3 transparent ceramic pumped by VBG diode **a** for various output coupler transmissions with sample temperature of 80 K and **b** for various sample temperatures with $T_{oc} = 30\%$

detrimental at the cryogenic temperature (80 K) [7]. The laser output wavelength was centered around 1932 nm, irrespective of the T_{oc} used, as shown in Fig. 8a. In comparison to the broadband diode-pumped laser (Fig. 6a), this VBG diode-pumped laser shows clearly improved performance due to a better wavelength and bandwidth matching between the sample absorption and pump emission. An absorption of 62% was measured under non-lasing condition. Thus, it is crucial for the laser design to optimize the emission wavelength and bandwidth of the pump source to match the absorption peak.

With T_{oc} fixed at 30%, the laser performance was characterized by varying the sample temperature. The sample temperature was limited up to 180 K to avoid the sample damage. The incident/output power characteristics are shown in Fig. 7b, where a clear effect of the sample temperature on the laser output and slope efficiency is observed. This trend could be due to the influence of reabsorption and parasitic processes arising at higher temperatures. The laser threshold increases with temperature, while the maximum output power and slope efficiency decrease. The output laser wavelength measured for different sample temperatures was centered at 1932 nm (see Fig. 8b).

With the measured absorption of 62%, we plotted the absorbed/output power characteristic in comparison with the incident/output power characteristic (as illustrated in Fig. 9a). The maximum output power of 6.4 W was achieved at an absorbed pump power of 12.7 W, which gives an optical-to-optical efficiency of 50.4%. The slope efficiency with respect to the absorbed power amounts to 52.0%. The laser beam is shown in Fig. 9b, which is a very-high-quality far field Gaussian beam profile obtained under an absorbed pump power of 9.2 W, corresponding to the output power of 4.7 W.

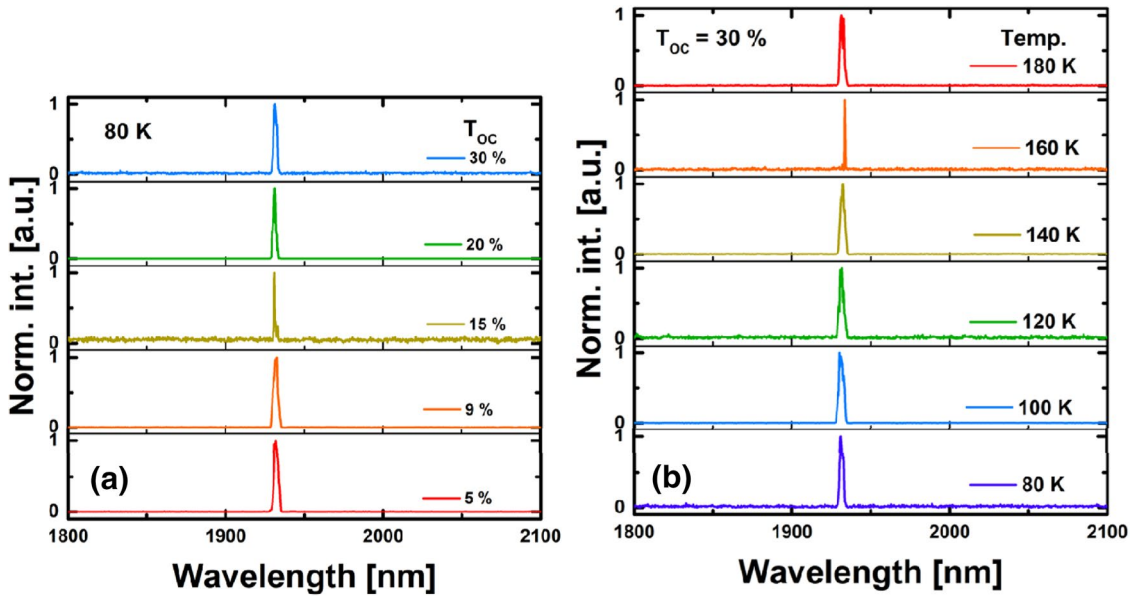

Fig. 8 Laser wavelength for **a** various output coupling transmissions at 80 K and **b** for various sample temperatures using 30% output coupler

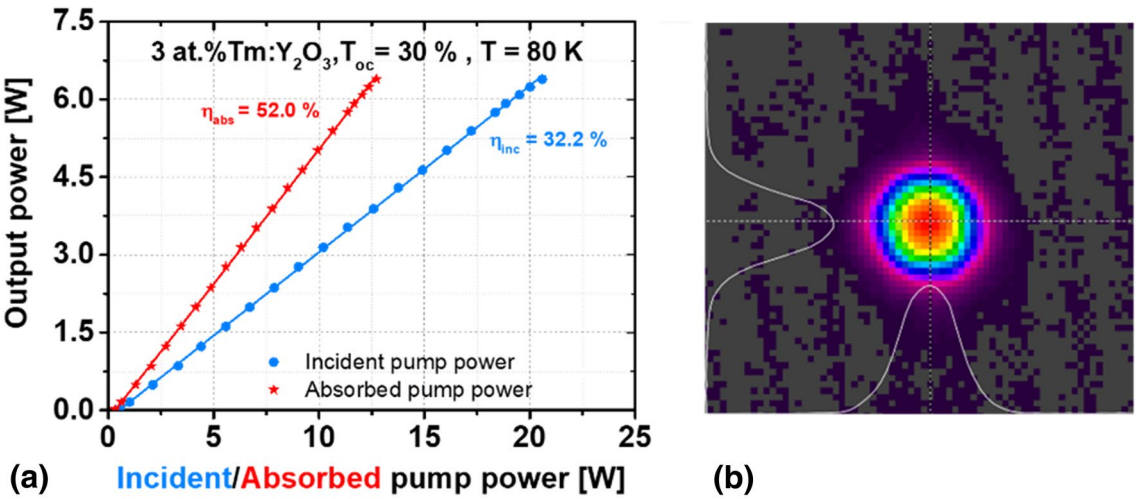

Fig. 9 Laser performance of the 3 at.% Tm:Y_2O_3 transparent ceramic pumped by VBG diode at 80 K with T_{oc} = 30%: **a** output power versus incident (blue dots)/absorbed pump power (red dots); **b** far field beam Gaussian profile

4 Conclusions

In this work, we presented the cryogenic spectroscopic and laser characteristics of a 3 at.% Tm:Y_2O_3 transparent ceramic. Absorption, emission and gain cross sections were estimated for various temperatures using the theoretical methods. Strong absorption bands are observed at 793 nm and 797 nm matching with the emission wavelength of AlGaAs laser diodes. An absorption cross section of 4.7×10^{-21} cm^2 with a bandwidth of 0.7 nm centered at 793.3 nm and an emission cross section of 29.0×10^{-21} cm^2 centered at 1930.9 nm were estimated at 80 K. We also studied the laser performance using broadband and VBG stabilized laser diodes emitting around 793 nm as pump sources. The best laser performance was achieved using the VBG stabilized pump source, which confirms the need of optimizing the pump wavelength and bandwidth for the laser design. A maximum output power of 6.4 W was achieved at 80 K with a slope efficiency of 52.0% with respect to the absorbed power. An excellent performance along with a good beam quality verifies the advantages of cryogenic cooling and VBG stabilized diode pumping. Future work will be focused on using samples of higher dopant concentrations to

achieve higher output and using other VBG pump sources to better match the absorption peak of Tm:Y_2O_3. Consequently, HAPP lasers will be designed using Tm:Y_2O_3 transparent ceramics.

Acknowledgements This work was co-financed by the European Regional Development Fund and the state budget of the Czech Republic (Project HiLASE CoE: Grant No. CZ.02.1.01/0.0/0.0/15_006/0000674) and by the European Union's Horizon 2020 research and innovation program under grant agreement No. 739573. This work was also supported by the Ministry of Education, Youth and Sports of the Czech Republic (Programmes NPU I Project No. LO1602, and Large Research Infrastructure Project No. LM2015086).

References

1. K.T. Zawilski, S.D. Setzler, P.G. Schunemann, T.M. Pollak, J. Opt. Soc. Am. B **23**, 2310–2316 (2006)
2. G.J. Wagner, T.J. Carrig, R.H. Page, K.I. Schaffers, J. Ndap, X. Ma, A. Burger, Opt. Lett. **24**, 19–21 (1999)
3. C.R. Phipps, K.L. Baker, B. Bradford, E.V. George, S.B. Libby, D.A. Liedahl, B. Marcovici, S.S. Olivier, L.D. Pleasance, J.P. Reilly, A. Rubenchik, D.N. Strafford, M.T. Valley, Adv. Space Res. **49**, 1283–1300 (2012)
4. I. Mingareev, F. Weirauch, A. Olowinsky, L. Shah, P. Kadwani, M. Richardson, Opt. Laser Technol. **44**, 2095–2099 (2012)
5. K. Scholle, P. Fuhrberg, P. Koopmann, S. Lamrini, 2 µm laser sources and their possible applications, in *Frontiers in Guided Wave Optics and Optoelectronics, Ch. 21*, ed. by B. Pal (INTECH Open Access Publisher, Rijeka, 2010)
6. A. Godard, C R Phys. **8**, 1100–1128 (2007)
7. P. Loiko, P. Koopmann, X. Mateos, J.M. Serres, V. Jambunathan, A. Lucianetti, T. Mocek, M. Aguilo, F. Diaz, U. Griebner, V. Petrov, C. Kraenkel, IEEE J. Sel. Top. Quantum Electron. **24**, 1–13 (2018)
8. D.C. Brown, S. Tornegard, J. Kolis, C. McMillen, C. Moore, L. Sanjeewa, C. Hancock, Appl. Sci. **6**, 23 (2016)
9. C. Kraenkel, IEEE J. Sel. Top. Quantum Electron. **21**, 250–262 (2015)
10. J. Szela, K.A. Sloyan, T.L. Parsonage, J.I. Mackenzie, R.W. Eason, Opt. Express **21**, 12460–12468 (2013)
11. H. Huang, H. Wang, D. Shen, Opt. Mater. Express **7**, 3147–3154 (2017)
12. P. Koopmann, S. Lamrini, K. Scholle, P. Fuhrberg, K. Petermann, G. Huber, Opt. Lett. **36**, 948–950 (2011)
13. P.A. Ryabochkina, A.N. Chabushkin, Y.L. Kopylov, V.V. Balashov, K.V. Lopukhin, Quantum Electron. **46**, 597–600 (2016)
14. H. Wang, H. Huang, P. Liu, L. Jin, D. Shen, J. Zhang, D. Tang, Opt. Mater. Express **7**, 296–303 (2017)
15. J. Körner, V. Jambunathan, J. Hein, R. Seifert, M. Loeser, M. Siebold, U. Schramm, P. Sikovinski, A. Lucianetti, T. Mocek, M.C. Kaluza, Appl. Phys. B **116**, 75–81 (2014)
16. D.E. McCumber, Phys. Rev. **136**, A954–A957 (1964)
17. W. Koechner, *Solid-State Laser Engineering* (Springer, New York, 1986), p. 17
18. S.A. Payne, L.L. Chase, L.K. Smith, W.L. Kway, W.F. Krupke, Infrared cross-section measurements for crystals doped with Er^{3+}, Tm^{3+}, Ho^{3+}. IEEE J. Quantum Electron. **28**, 2619–2630 (1992)
19. J. Koerner, T. Lühder, J. Reiter, I. Uschmann, H. Marschner, V. Jambunathan, A. Lucianetti, T. Mocek, J. Hein, M.C. Kaluza, J. Lumin. **202**, 427–437 (2018)
20. R.P. Leavitt, J.B. Gruber, N.C. Chang, C.A. Morrison, J. Chem. Phys. **76**, 4775–4788 (1982)
21. J. Sanghera, W. Kim, G. Villalobos, B. Shaw, C. Baker, J. Frantz, B. Sadowski, I. Aggarwal, Materials **5**, 258–277 (2012)